Electronic Supplementary Material (ESI) for Inorganic Chemistry Frontiers.


# Supplementary Information

## Highly dispersed ultra-small $RuO_2$ nanoparticles on NiO nanosheets arrays as efficient pH-universal hydrogen evolution electrocatalysts

Dongdong Du[a], Yiyun Du[b], Yongjun Feng[a], Dianqing Li[a, *], and Pinggui Tang[a, *]

[a] State Key Laboratory of Chemical Resource Engineering, and Beijing Engineering Center for Hierarchical Catalysts, Beijing University of Chemical Technology, Beijing 100029, P.R. China

[b] State Nuclear Electric Power Planning Design & Research Institute Co., Ltd., State Nuclear Power Technology Corporation: SPIC, Beijing 100095, China

*Corresponding authors.

E-mail addresses: lidq@mail.buct.edu.cn (D. Li), tangpg@mail.buct.edu.cn (P. Tang).

## 1. Experimental

### *1.1. Reagents*

Ruthenium chloride trihydrate ($RuCl_3 \cdot 3H_2O$), sodium chloride (NaCl), nickel chloride hexahydrate ($NiCl_2 \cdot 6H_2O$), hydrochloric acid (HCl), ethanol ($C_2H_6O$) and urea were analytically pure and purchased from Sinopharm Chemical Reagent Co., Ltd. Nickel foam (NF) with a thickness of 1.6 mm was obtained from Suzhou Taili Materials Technology Co., Ltd.. Deionized water was used for the preparation of solutions.

### *1.2. Synthesis of $RuO_2/NiO_2$/NF nanosheet array*

Typically, a piece of NF with size of 4.0 × 5.0 $cm^2$ was treated in a 6 M HCl solution for 15 min to remove the nickle oxide layer, and then sonicated in ethanol and deionized water for 15 min, respectively, followed by washing with deionized water for several times. $NiCl_2 \cdot 6H_2O$ (0.16 mmol), $RuCl_3 \cdot 3H_2O$ (0.08 mmol) and NaCl (0.163 mol) were dissolved in 80 mL of deionizd water to form a solution with magnetic stirring. A piece of cleaned NF was immersed into the solution and the reaction was carried out in a water bath shaker at 80 °C for 6 h. The obtained $RuO_2/Ni(OH)_2$/NF nanosheet array was washed with deionized water and ethanol for several times before drying at room temperature, and was named as $Ni_2Ru(OH)_x$. Precursors of $Ni_0Ru(OH)_x$, $Ni_1Ru(OH)_x$, $Ni_3Ru(OH)_x$, $Ni_4Ru(OH)_x$ and $Ni(OH)_2$ were also synthesized by changing the Ni : Ru molar ratio to be 0 : 1, 1 : 1, 3 : 1, 4 : 1 and 1 : 0, respectively, according to the same method. The obtained precursors were subsequently calcined at

300 °C for 1 h at air atmosphere in a muffle oven to prepare catalysts of $Ni_0RuO_x$, $Ni_1RuO_x$, $Ni_2RuO_x$, $Ni_3uO_x$, $Ni_4RuO_x$ and NiO, respectively.

*1.3. Synthesis of $RuO_2$ and Pt/C*

The powdered $RuO_2$ was prepared by a precipitation method using KOH as the precipitant. Typically, 1.0 mL KOH (1.0 M) solution was added dropwise into 100 mL of $RuCl_3$ solution (0.01 M) under magnetic stirring, followed by aging at 100 °C for 45 min. The precipitates were collected and washed with deionized water for several times and dried at 60 °C for 12 h. For comparison, $RuO_2$ and commercial Pt/C catalysts were prepared by drop-casting their powdered forms on NF as follows: 10.0 mg of catalyst powder was dispersed into a mixture consisting of 10 μL of Nafion solution and 990 μL of ethanol/water solution with volume ratio of 1 : 1 by ultrasonic treatment for 60 min to form a homogeneous ink. Subsequently, 200 μL of catalyst ink was loaded on a piece of NF (1×1 $cm^2$) with a mass loading of 2 mg $cm^{-2}$ at room temperature.

*1.4. Characterizations*

The XRD patterns of the catalysts were recorded using an X-ray diffractometer with Ni-filtered Cu-Kα radiation (Rigaku D/max-Ultima III). The morphology and structure of the catalysts were characterized by a scanning electron microscope (Zeiss Supra 55) and a high-resolution transmission electron microscopy (JEOL JEM-2010 with an accelerating voltage of 200 kV). The high-angle annular dark-field scanning transmission electron microscopy (HAADF-STEM) and energy-dispersive spectroscopy (EDS) mapping analyses were executed on a JEOL JEM-2014 electron

microscopy (Tokyo, Japan). The X-ray photoelectron spectroscopy (XPS) analysis was performed on an ESCALAB 250 X–ray photoelectron spectrometer using Al-Kα radiation. The inductively coupled plasma atomic emission spectra (ICP-AES) were used to determine the content of Ru element in the catalysts.

*1.5. Electrochemical Measurements*

The electrochemical measurements was performed in a conventional three-electrode cell in a water bath at 25 °C. The $RuO_2$/NiO/NF nanosheet array was tailored into size of 1 × 1 $cm^2$ and used as the working electrode for the HER tests. A Hg/HgO electrode served as the reference electrode in 1.0 M KOH (pH=14) while $Hg_2Cl_2$(s)|Hg(l) was used in 0.5 M $H_2SO_4$ (pH=0) and 1.0 M PBS (pH=7), and a graphite rod served as the counter electrode. The potential was normalized to reversible hydrogen electrode (RHE) by the following Nernst equations.

1.0 M KOH: $E_{vs.RHE} = E_{vs.Hg/HgO} + E^{\theta}_{vs.Hg/HgO} + 0.8274$

0.5 M $H_2SO_4$: $E_{vs.RHE} = E_{vs.Hg_2Cl_2/Hg(l)} + E^{\theta}_{vs.Hg_2Cl_2/Hg(l)}$

1.0 M PBS: $E_{vs.RHE} = E_{vs.Hg_2Cl_2/Hg(l)} + E^{\theta}_{vs.Hg_2Cl_2/Hg(l)} + 0.4137$

All electrolytes were bubbled with Ar for 30 min before HER measurements. The working electrodes were first activated by cyclic voltammetry (CV) scans till stabilization with a scan rate of 50 mV $s^{-1}$. The linear-sweep voltammetry (LSV) curves were recorded at a scan rate of 5 mV $s^{-1}$ with 90% iR-correction to compensate the resistances drops, and the current density was normalized to the geometric area. Electrochemical impedance spectroscopy (EIS) measurements were performed by using an AC voltage with 10 mV amplitude in the frequency range of 100000-0.01 Hz.

The long-term durability was tested by CV scans for 3000 cycles with a scan rate of 100 mV $s^{-1}$, and the long-term stability was evaluated by chronoamperometry at 100 mA $cm^{-2}$ for 200 h.**The electrochemically active surface area**

The electrochemically active surface area (ECSA) was measured by double-layer charging ($C_{dl}$). The potential was set between 0.2 V to 0.30 V vs RHE ten time at different scan rates of 5 mV $s^{-1}$, 10 mV $s^{-1}$, 15 mV $s^{-1}$, 20 mV $s^{-1}$,25 mV $s^{-1,}$ 30 mV $s^{-1}$. By plotting $\Delta J = (J_a - J_c)/2$ against the scan rate, $C_{dl}$ was obtained from the slope. The specific capacitance value for a flat standard with 1 $cm^2$ of real surface area seen generally as in the range of 20-60 μF $cm^{-2}$, most using the 40 μF $cm^{-2.1,\ 2}$ The electrochemically active surface area (ECSA) was converted from the specific capacitance value by

$$A_{ECSA} = \frac{C_{dl}}{C_s} = \frac{C_{dl}}{40\ \mu F\ cm^{-2}}$$

**Faradaic efficiency**

And the Faradaic efficiency was obtained by the ratio of the volume of experimentally gas to volume calculated theoretically at the current density of 200 mA $cm^{-2}$, and theoretical gas volume was calculated by the following equation:[3, 4]

$$\eta = (V_{experimental}/V_{theoretical}) \times 100\%$$

$$V_{theoretical} = ItV_m/nF$$

η is Faradaic efficiency; F is Faraday's constant (96485.33 C $mol^{-1}$)，n is the amount of substance (mol); V is the gas volume (L); $V_m$ is the molar volume of gas $mol^{-1}$; I is current (A); t is time (min).

**TOF**

It is noting that the TOF calculations are roughly accurate because the number of active sites and the nature of active sites were not definite. TOF is calculated based on the assumption that $RuO_2$ acts as the active site,[5,6] because $Ni_2RuO_x$ show excellent activity far more than NiO. TOF values was calculated by the following formula:

$$TOF(s^{-1}) = \frac{\text{total hydrogen turnover/geomrtric area } (cm^2)}{\text{active sitres/geomrtric area } (cm^2)}$$

$$TOF(s^{-1}) = \frac{A \times |J|}{2 \times F \times n}$$

where J (A $cm^2$) is the current density at a given overpotential, A (1 $cm^2$) is geometric surface area of the working electrode, F is Faraday constant (96485 C $mol^{-1}$), n is the number of the active site.

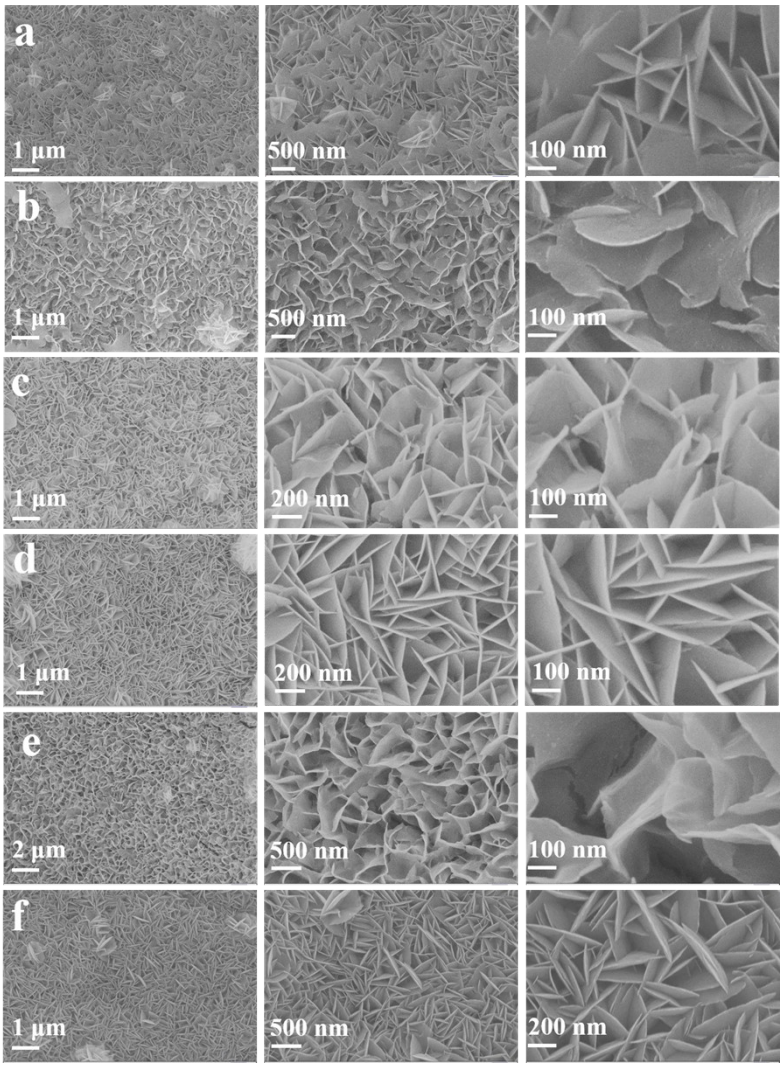


**Figure S1.** SEM images of a) $Ni_0Ru(OH)_x$, b) $Ni_1Ru(OH)_x$, c) $Ni_2Ru(OH)_x$, d) $Ni_3Ru(OH)_x$, e) $Ni_4Ru(OH)_x$ and f) $Ni(OH)_2$.

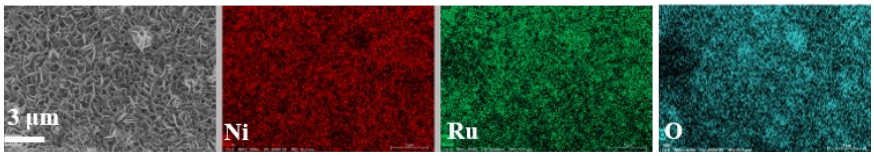


**Figure S2.** SEM images and elemental mapping of $Ni_2Ru(OH)_x$.

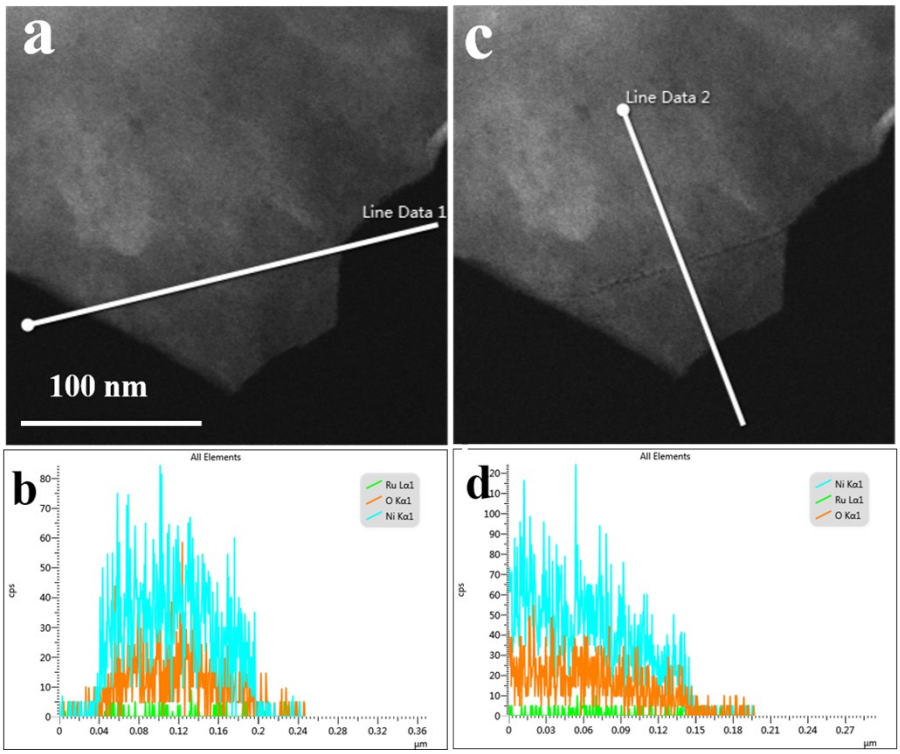


**Figure S3.** (a, c) HAADF-STEM image and (b, d) corresponding linear scanning curves of $Ni_2Ru(OH)_x$, respectively.

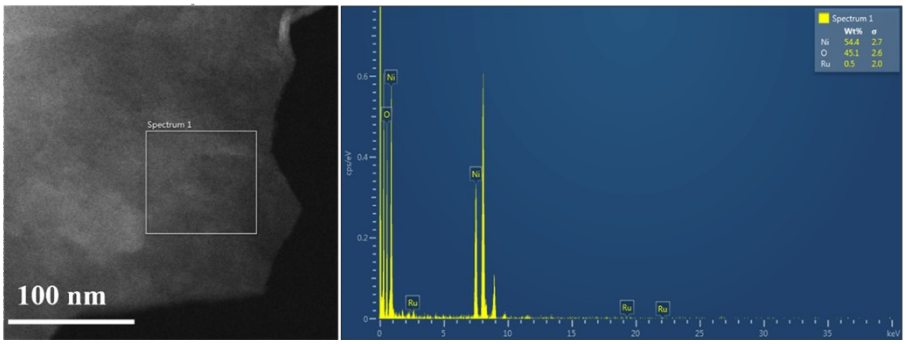


**Figure S4.** EDS spectrum of $Ni_2Ru(OH)_x$.

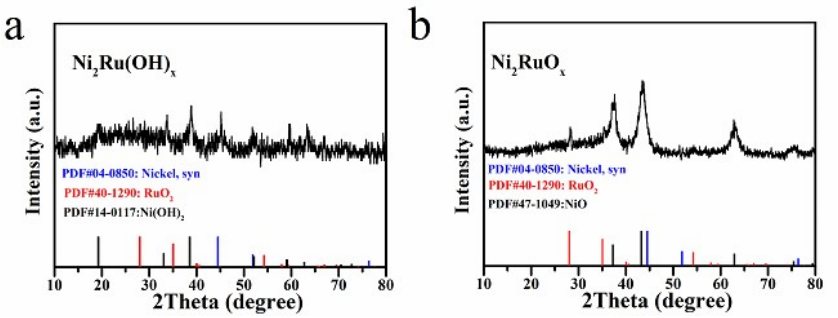


**Figure S5.** a) XRD pattern of $Ni_2Ru(OH)_x$ and b) $Ni_2RuO_x$.

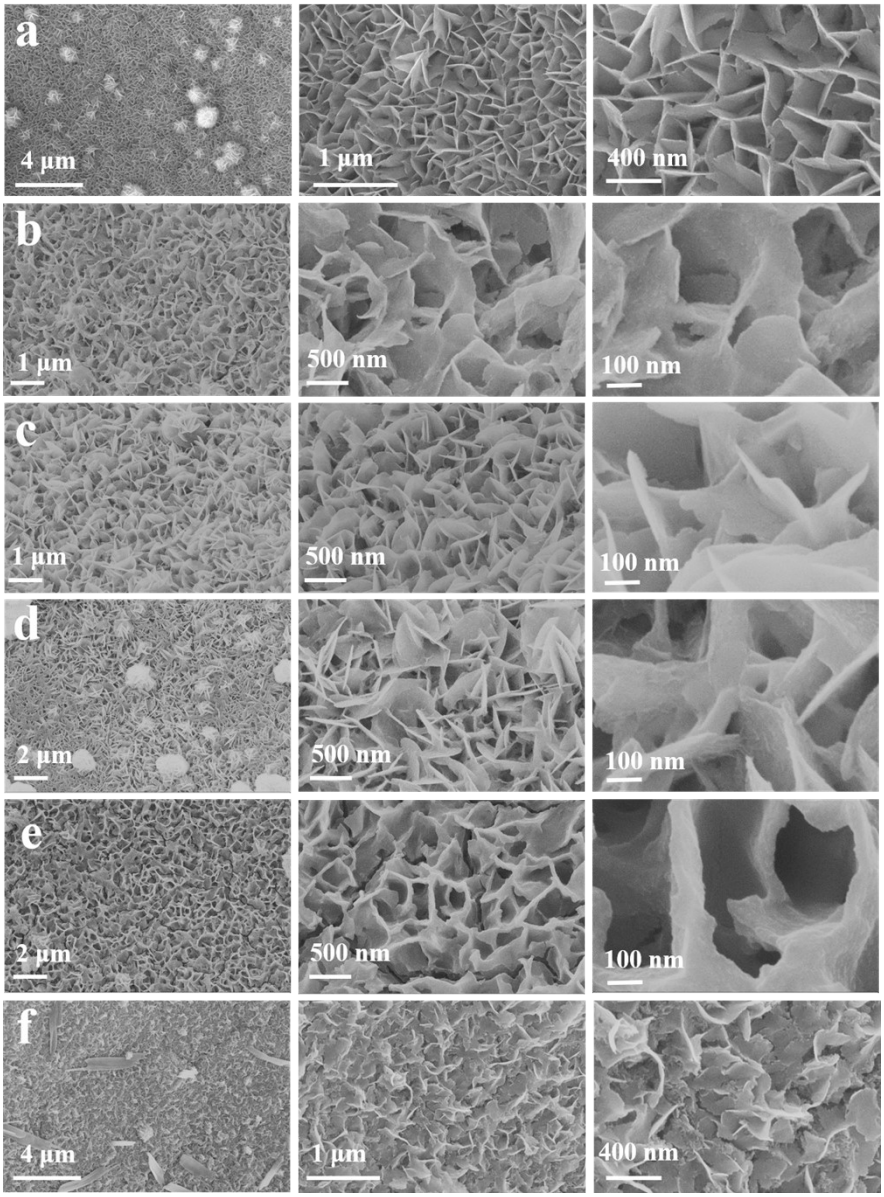


**Figure S6.** SEM images of a) $Ni_0RuO_x$, b) $Ni_1RuO_x$, c) $Ni_2RuO_x$, d) $Ni_3RuO_x$, e) $Ni_4RuO_x$ and f) NiO.

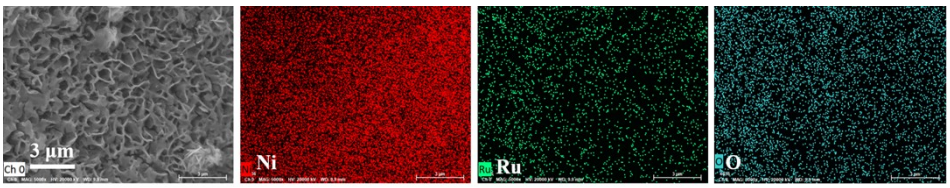


**Figure S7.** SEM image with elemental mapping of $Ni_2RuO_x$.

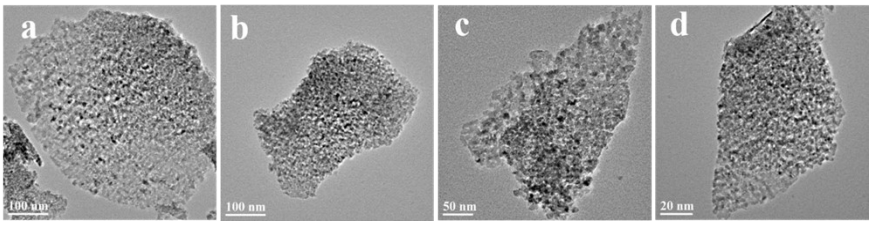


**Figure S8.** TEM images of $Ni_2RuO_x$.

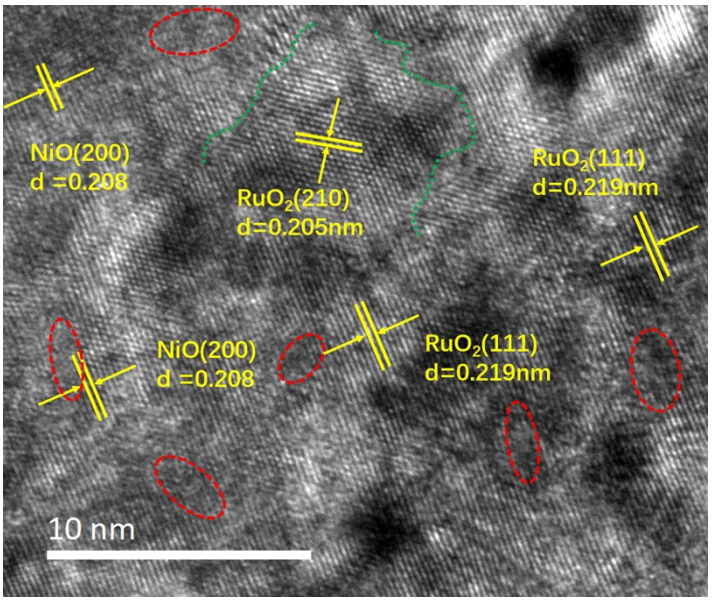


**Figure S9.** HRTEM images of $Ni_2RuO_x$.

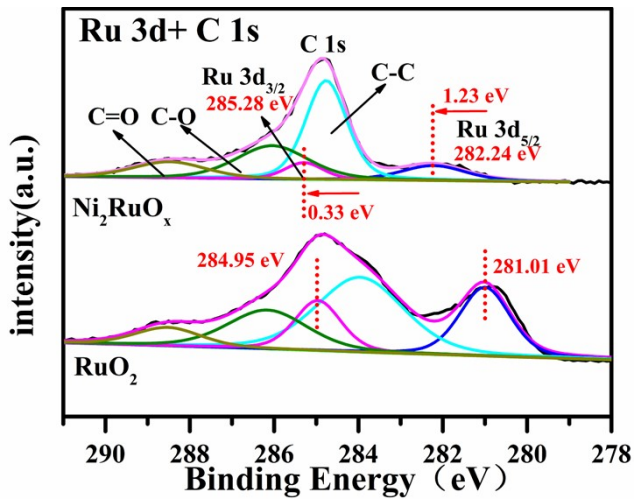


**Figure S10.** XPS spectra of Ru 3d+C1s of $Ni_2RuO_x$.

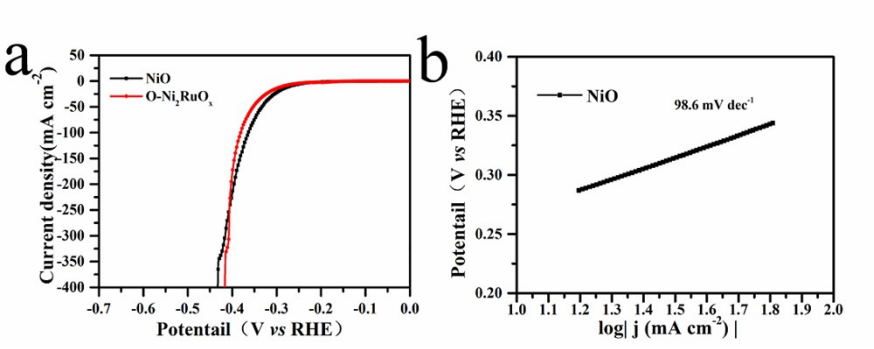


**Figure S11.** a) The iR-corrected polarization curves of catalysts measured in 1.0 M KOH and b) the corresponding Tafel plots of NiO.

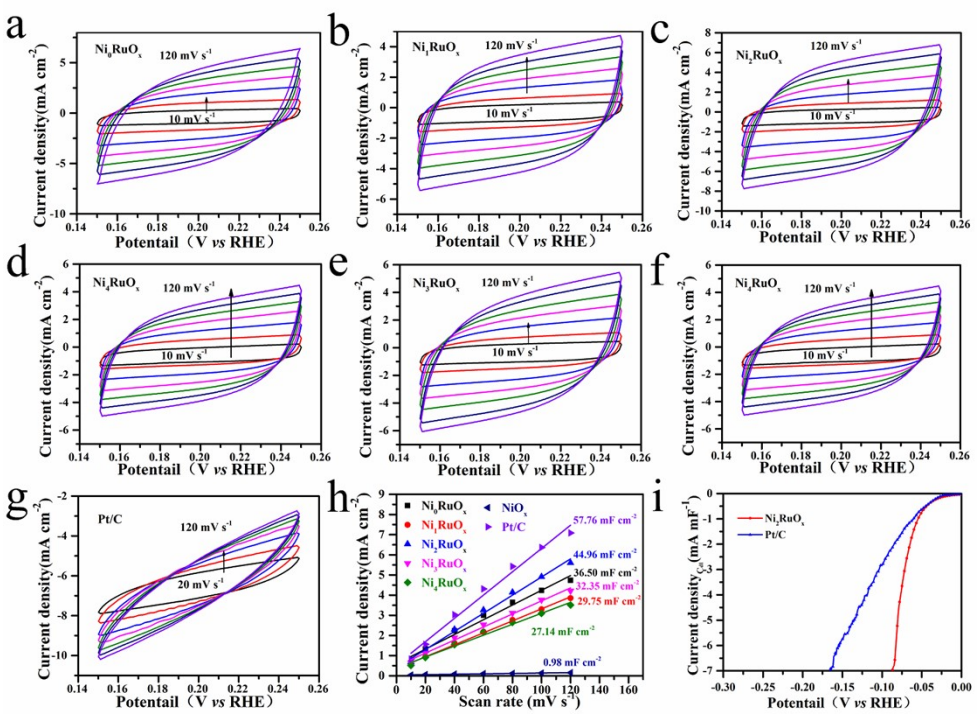


**Figure S12.** CV curves of a) $Ni_0RuO_x$, b) $Ni_1RuO_x$, c) $Ni_2RuO_x$, d) $Ni_3RuO_x$, e) $Ni_4RuO_x$, f) NiO, and g) Pt/C; h) Current density differences plotted against scan rates of catalysts; i) Polarization curves of normalized by $C_{dl}$ in 1M KOH.

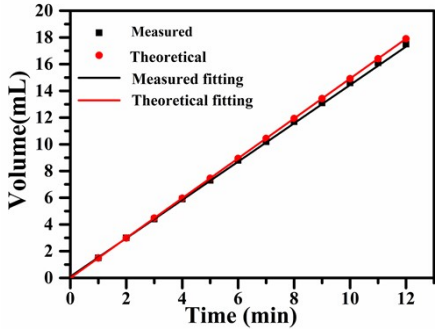


**Figure S13.** Faradaic efficiency of $Ni_2RuO_x$ in 1M KOH.

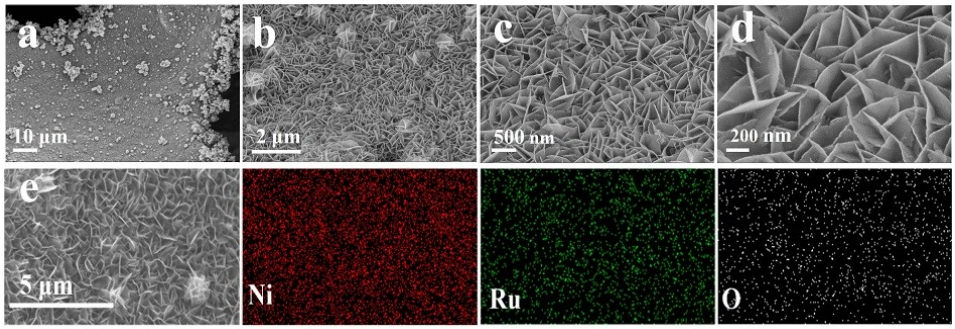


**Figure S14** a-d) SEM images and e) mapping of $Ni_2RuO_x$ after 200 h test at initial current density of 100 mA $cm^{-2}$ in 1M KOH.

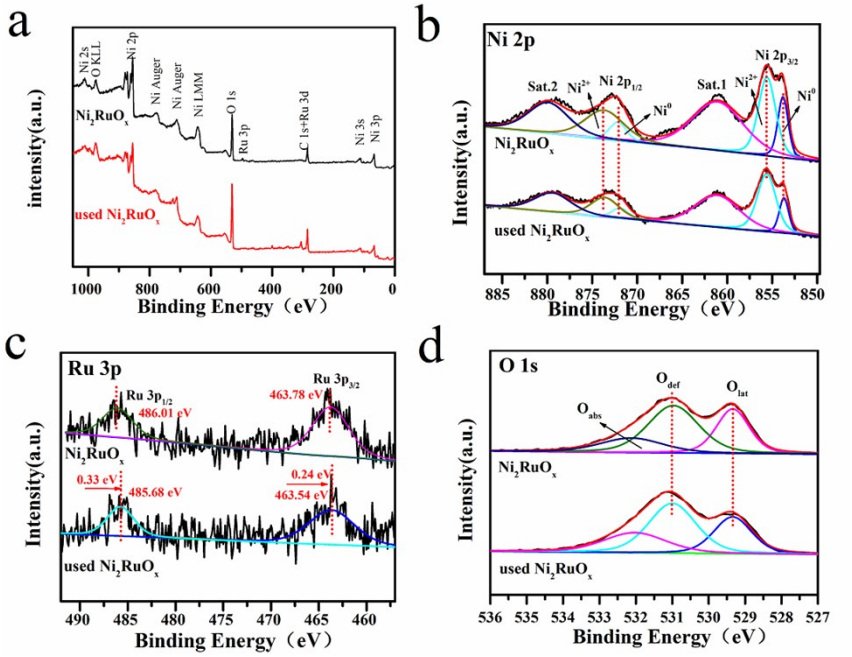


**Figure S15.** XPS spectra of before and 200 h test at initial current density of 100 mA $cm^{-2}$ in 1M KOH: a) overall XPS survey spectra, b) XPS spectra of Ni 2p, c) XPS spectra of Ru 3p and d) XPS spectra of O 1s.

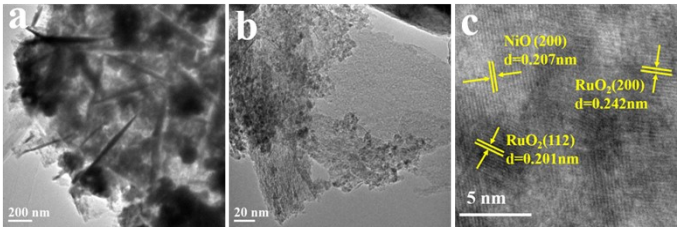


**Figure S16.** a-b) TEM images, c) HRTEM images of $Ni_2RuO_x$ after 200 h test at initial current density of 100 mA $cm^{-2}$ in 1M KOH.

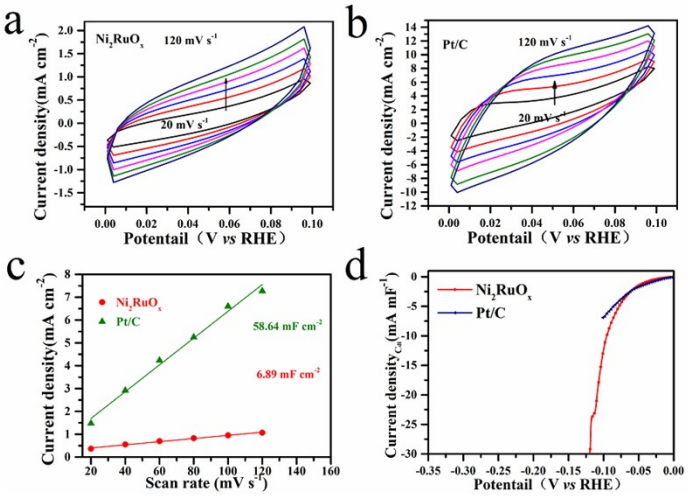


**Figure S17.** CV curves of a) $Ni_2RuO_x$ and b) Pt/C; c) Current density differences plotted against scan rates of catalysts; d) Polarization curves of normalized by $C_{dl}$ in 0.5M $H_2SO_4$.

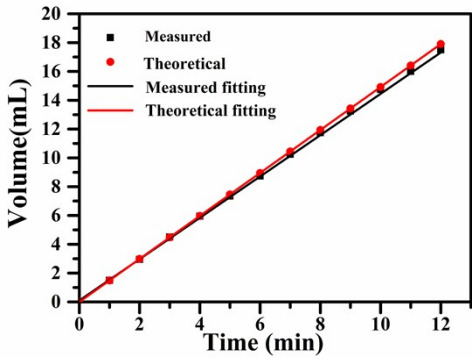


**Figure S18.** Faradaic efficiency of $Ni_2RuO_x$ in 0.5M $H_2SO_4$.

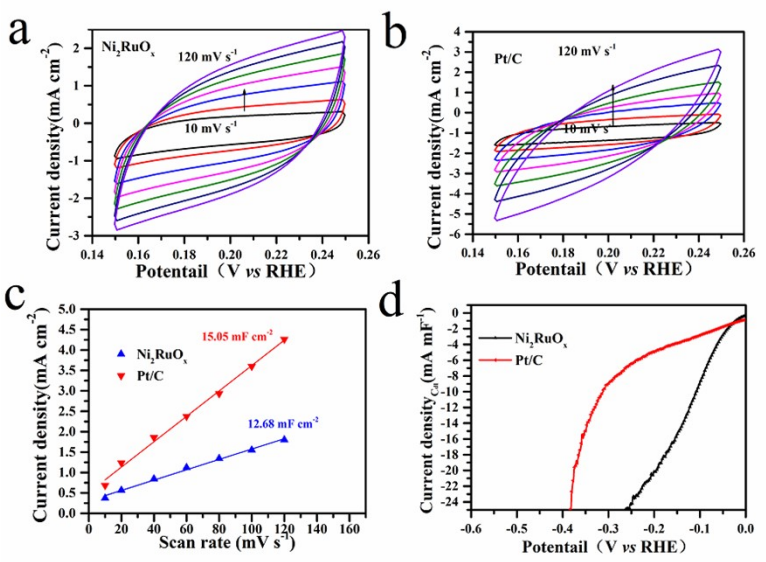


**Figure S19.** CV curves of a) $Ni_2RuO_x$ and b) Pt/C; c) Current density differences plotted against scan rates of catalysts; d) Polarization curves of normalized by $C_{dl}$ in 1M PBS

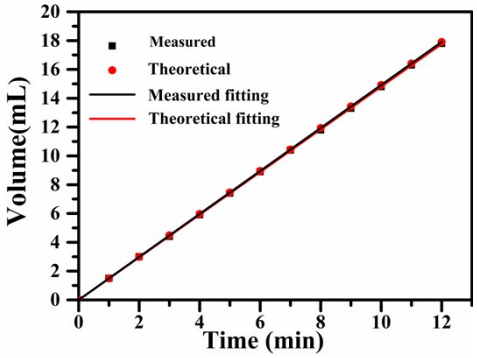


**Figure S20.** Faradaic efficiency of $Ni_2RuO_x$ in 1M PBS.

**Table S1.** Comparison of reported electrocatalysts for HER in 1 M KOH electolyte

| Catalysts | Catalyst amount (mg $cm^{-2}$) | Electrode area ($cm^2$) | *J* (mA $cm^{-2}$) | *η* (vs RHE) | Reference |
|---|---|---|---|---|---|
| **$Ni_2RuO_x$** | **0.165 (Ru)** | **1** | **10**<br>**100**<br>**300** | **31 mV**<br>**66 mV**<br>**84 mV** | **This work** |
| $NiFe_2O_4$/NiFe LDH | 2.8 | 0.25 | 10<br>100<br>500<br>750 | 101 mV<br>229 mV<br>297 mV<br>314 mV | ACS Appl. Mater. Interfaces, **2018**, 10, 26283-26292 |
| $Ni_{cluster}$–Ru NWs | 0.25 | 0.196 | 10 | 194 mV | Energy Environ. Sci, **2021**, 14, 3194 |
| $NiMoO_x$/NiMoS | | 1 | 10<br>100<br>500<br>1000 | 38 mV<br>89 mV<br>174 mV<br>236 mV | Nat. Commun, **2020**, 11, 5462 |
| Ni-Fe NP | 2.5 | - | 10 | 46 mV | Nat. Commun, **2019**, 10, 5599 |
| h-NiMoFe | 0.15 | - | 10<br>100<br>500<br>1000 | 14 mV<br>~ 50 mV<br>74 mV<br>98 mV | Energy Environ. Sci, **2021**, 14, 4610-4619 |
| NiMoN@NiFeN | | 1 | 100<br>500 | 84 mV<br>180 mV | Nat. Commun, **2019**, 10, 5106 |
| $Ni_2P/NiTe_2$ | | - | 10<br>100 | 62 mV<br>143 mV | Energy Environ. Sci, **2020**, 13, 1799-1807 |
| Ni@NCNT/NiMN/NF | 41.3 | 1 | 10<br>100<br>300 | 15 mV<br>~120 mV<br>~180 mV | J. Mater. Chem. A, **2019**, 7, 13671–13678 |
| Pt–Ni NTAs | 1.516 | - | 10<br>200 | 23 m V<br>71 mV | Energy Environ. Sci, **2021**, 14, 1594 |

| | | | | | |
|---|---|---|---|---|---|
| NiO/Ru@Ni | - | - | 10 | 39 mV | J. Mater. Chem. A, **2019**, 7, 2344 |
| Fe-$Ni_3S_2$/NF | 4~6 | - | 10<br>100 | 47 mV<br>232 mV | ACS Catal, **2018**, 8, 5431-5441 |
| NF@$Fe_2$-$Ni_2P$/C | | 0.5 | 10<br>100<br>300<br>1000 | 39 mV<br>~80 mV<br>~95 mV<br>183 mV | ACS Catal, **2019**, 9, 8882-8892 |
| $CoO_x$-$RuO_2$/NF | 0.138% wt(Ru) | 0.4 | 50<br>100<br>300<br>1500 | 51 mV<br>~100 mV<br>~120 mV<br>215 mV | ACS Sustainable Chem. Eng, **2020**, 8, 47 |
| $Ni_3N$-VN/NF | | 1 | 10<br>100 | 73 mV<br>320 mV | Adv. Mater, **2019**, 31, 1901174 |
| CuNi@NiFeCu | | 1 | 10<br>100<br>300 | 98 mV<br>~ 280 mV<br>300 mV | Appl. Catal. B Environ., **2021**, 298, 120600 |
| C-350 | 0.35 | 0.25 | 10 | 47mV | ACS Sustainable Chem. Eng, **2020**, 8, 7414-7422 |
| Ni@$Ni_2P$-Ru HNRs | 0.35 | 0.07065 | 10<br>50 | 31 mV<br>~ 200 mV | J. Am. Chem. Soc, **2018**, 140, 2731-2734 |
| Ru@CN-0.16 | 3.14 % wt(Ru) | 0.19625 | 10<br>50 | 32 mV<br>~135 mV | Energy Environ. Sci, **2018**, 11, 800 |
| $Ru_2Ni_2$ SNs/C | - | - | 10<br>20 | 40 mV<br>55 mV | Nano Energy, **2018**, 47, 1−7 |
| $RuP_2$@NPC | 0.1 | 0.07065 | 10<br>50 | 52 mV<br>~ 115 mV | Angew. Chem. Int. Ed, **2017**, 56, 11559–11564 |
| Ni-Co-P HNBs | 2 | 1 | 10<br>100 | 107 mV<br>187 mV | Energy Environ. Sci, **2018**, 11, 872–880 |
| Ni-P-B/NF | | 0.5 | 50<br>500 | 76 mV<br>251 mV | Energy Environ. Sci, **2020**, 13, 102–110 |
| hydrous $RuO_2$ | 0.52 | 1 | 10 | 60 mV | Chem. Phys. Lett. **2017**, |

| | | | | | |
|---|---|---|---|---|---|
| | | | 100 | 184 mV | 673, 89−92 |
| Cu@NiFe LDH | 2.2 | - | 10 | 116 mV | Energy Environ. Sci, |
| | | | 100 | 192 mV | **2017**, 10, 1820–1827 |
| Ni-Fe-$K_{0.23}MnO_2$ | 2 | 1 | 10 | 114 mV | Small, **2020**, 16, |
| CNFs-300 | | | 100 | 244 mV | 1905223 |
| $NiCo_2O_4$@$NiMo_2$ | 2.6 | 0.785 | 10 | 157 mV | Adv. Mater. Interfaces, |
| $S_4$ | | | 100 | 289 mV | **2019**, 6, 1901308 |
| | | | 300 | 343 mV | |
| Pt-SL/$TiO_2$ | 0.00286 | 0.1767 | 10 | 205 mV | Small, **2021**, 17, |
| | | | | | 2100732 |
| CoP@$Ni_2P$ | 4 | 0.25 | 10 | 16 mV | Appl. Catal. B Environ., |
| | | | 100 | 85 mV | **2021**, 296, 120350 |
| | | | 300 | ~150 mV | |

**Table S2.** Comparison of reported electrocatalysts for HER in 0.5 M $H_2SO_4$ electolyte

| **Catalysts** | **Catalyst amount (mg cm$^{-2}$)** | **Electrode area (cm$^2$)** | ***J* (mA cm$^{-2}$)** | ***η* (vs RHE)** | **Reference** |
|---|---|---|---|---|---|
| **$Ni_2RuO_x$** | **0.165** | **1** | **10** | **18 mV** | |
| | **(Ru)** | | **100** | **95 mV** | **This work** |
| | | | **300** | **253 mV** | |
| NiMo-NGTs | 2 | 0.07065 | 10 | 65 mV | ACS Nano, **2016**, 10, |
| | | | 100 | 205 mV | 10397–10403 |
| Ni@$Ni_2P$–Ru | - | 0.07065 | 10 | 51 mV | J. Am. Chem. Soc, **2018**, |
| | | | 50 | ~100 mV | 140, 2731−2734 |
| PtLa@KB | - | 0.07065 | 10 | 38 mV | Small, **2021**, 17, 2102879 |
| | | | 100 | 100 mV | |
| ECM@Ru | - | - | 10 | 63 mV | Adv. Energy Mater, **2020**, |
| | | | 50 | 102 mV | 10, 2000882 |
| [Ru(SA)+Ru(NP) | - | 0.07065 | 10 | 10 mV | Adv. Energy Mater, **2019**, |

| | | | | | |
|---|---|---|---|---|---|
| @RuNx@GN]/GN | | | | | 9, 1900931 |
| $Ru_{0.10}$@2HMoS$_2$ | - | - | 10<br>200 | 147 mV<br>~250 mV | Appl. Catal. B Environ., **2021**, 298,120490 |
| 1Ni-0.5Mo$_2$C/GNS | 0.38 | 1 | 10<br>100<br>300 | 50 mV<br>57 mV<br>~85 mV | Journal of Catalysis, **2020**, 388, 122-29 |
| Ru@C$_2$N | 0.285 | 0.07065 | 10 | 13.5 mV | Nature Nanotechnology, **2017**, 12, 441-446 |
| Ru SAs–Ni$_2$P | - | 0.196 | 10<br>100 | 125 mV<br>~200 mV | Nano Energy, **2021**, 80, 105467 |
| Ru$_x$Fe$_y$P-NC$_s$/CNF | 0.36 | 0.07065 | 10<br>100 | 151 mV<br>242 mV | Appl. Catal. B Environ., **2021**, 283, 119583 |
| Ni$_{cluster}$–Ru | 0.25 | 0.196 | 10 | 20 mV | Energy Environ. Sci, **2021**, 14, 3194–3202 |
| N-Co-S/G | - | 0.196 | 10<br>50 | 120 mV<br>~110 mV | Nano Energy, **2021**, 80, 105544 |
| Ru-SA/Ti $C_2T_x$ | 3.5wt% | 0.196 | 10 | 70 mV | Small, **2020**, 16, 2002888 |
| RuCu NSs/C | 5 | 0.196 | 10 | 19 mV | Angew.Chem. Int. Ed, **2019**, 58,13983 –13988 |
| Ir-SA@Fe@NCNT | 0.283 | 0.0765 | 10<br>500 | 26 mV<br>~340 mV | Nano Lett, **2020**, 20, 2120−2128 |
| Ir-NR/C | 0.283 | 0.0765 | 10<br>50 | 28 mV<br>~90 mV | Appl. Catal. B Environ., **2020**, 279, 119394 |
| RuIrZnO | 0.01 | 0.049 | 10 | 12 mV | Nat. Commun, **2019**, 10, 4875 |
| RuIr-NC | 0.05 | 0.196 | 10 | 46 mV | Nat. Commun, **2021**, 12, 1145 |
| NiVB/rGO | 0.56 | 0.0765 | 10<br>50 | 146 mV<br>~300 mV | Journal of Energy Chemistry, **2021**, 58,237-246 |
| S-MoP NPL | - | 0.785 | 10<br>100 | 85 mV<br>~160 mV | ACS Catal, **2019**, 9, 651−659 |
| MoS$_2$/NLG-3 | 0.293 | 0.15 | 10 | 110 mV | ACS Catal. **2021**, 11, |

| | | | | | |
|---|---|---|---|---|---|
| | | | 20 | 179 mV | 4486−4497 |
| | | | 100 | ~190 mV | |
| Ir NWs | 0.204 | 0.196 | 10 | 15 mV | Adv. Funct. Mater, **2018**, 28, 1803722 |

**Table S3.** Comparison of reported electrocatalysts for HER in 1 M PBS electolyte

| **Catalysts** | **Catalyst amount (mg cm$^{-2}$)** | **Electrode area (cm$^2$)** | ***j*** **(mA cm$^{-2}$)** | ***η*** **(vs RHE)** | **Reference** |
|---|---|---|---|---|---|
| **$Ni_2RuO_x$** | **0.165 (Ru)** | **1** | **10** | **16 mV** | |
| | | | **100** | **131 mV** | **This work** |
| | | | **300** | **289 mV** | |
| $Ru_{0.10}$@2H$MoS_2$ | - | - | 10 | 137 mV | Appl. Catal. B Environ., |
| | | | 50 | ~255 mV | **2021**, 298, 120490 |
| Ir-NSG | 0.3 | - | 10 | 22 mV | Nat. Commun, **2020**, 11, 4246 |
| Ir-NR/C | 0.283 | 0.0765 | 10 | 86 mV | Appl. Catal. B Environ., |
| | | | 50 | ~300 mV | **2020**, 279, 119394 |
| S-MoP NPL | - | 0.785 | 10 | 142 mV | ACS Catal, **2019**, 9, 651−659 |
| $MoS_2$/NLG-3 | 0.293 | 0.15 | 10 | 142 mV | ACS Catal, **2021**, 11, |
| | | | 20 | 167 mV | 4486−4497 |
| | | | 100 | ~200 mV | |
| CoP/Co-MOF | 5 | - | 10 | 49 mV | Angew.Chem. Int.Ed, **2019**, |
| | | | 100 | ~140 mV | 58,4679-4684 |
| Ni-$Ni_x$ | - | 0.25 | 10 | 64 mV | J. Am. Chem. Soc, **2017**, |
| | | | 100 | ~ 210 mV | 139, 12283-12290 |

| | | | | | |
|---|---|---|---|---|---|
| MoP700 | 0.25 | 0.196 | 10<br>100 | 196 mV<br>~ 225 mV | ACS Catal, **2019**, 9, 8712-8718 |
| $Ni_{0.1}Co_{0.9}P$ | 0.58 | - | 10 | 125 mV | Angew. Chem. Int. Ed, **2018**, 57,15445-15449 |
| $Ni_{0.89}Co_{0.11}Se_2$ | 2.62 | - | 10<br>100 | 82 mV<br>~313 mV | Adv. Mater, **2017**, 29, 1606521 |
| N–$Co_2P$/CC | 2 | 0.196 | 10<br>20 | 42 mV<br>~160 mV | ACS Catal, **2019**, 9, 3744-3752 |
| karst NF | 0.5 | 0.25 | 10<br>100 | 110 mV<br>~ 310 mV | Energy Environ. Sci, **2020**, 13, 174-182 |
| $CoS_x$-(0.2-0.02)-12 | 0.242 | 0.3 | 10<br>50 | 168 mV<br>282 mV | Adv. Funct. Mater, **2018**, 28, 1707244 |
| Mn–NiO–Ni/Ni–F | 0.25 | - | 10 | 80 mV | Energy Environ. Sci, **2018**, 11, 1898–1910 |
| Hollow $Ni(S_{0.5}Se_{0.5})2$ | 0.75 | 1 | 10<br>100 | 124 mV<br>~ 205 mV | J. Mater. Chem. A, **2019**, 7, 16793–16802 |
| $Ni_{12}P_5$-$Ni_2P$ | - | - | 10<br>100 | 112 mV<br>162 mV | Appl. Catal. B Environ., **2021**, 282, 119609 |
| np-$Co_9S_4P_4$ | 1 | - | 10 | 87 mV | ACS Appl. Mater. Interfaces, **2019**, 11, 3880-3888 |
| $Cu_{0.08}Co_{0.92}P$ | 5.17 | - | 10<br>50 | 81 mV<br>165 mV | Appl. Catal. B Environ., **2020**, 265, 118555 |
| $Co_{1-x}Fe_xP$/CNT | 0.5 | 0.5 | 10 | 105 mV | Adv. Funct. Mater, **2017**, 27, 1606635 |

## REFERENCES


(1) Kibsgaard, J.; Tsai, C.; Chan, K.; Benck, J. D.; Nørskov, J. K.; Abild-Pedersen, F.; Jaramillo, T. F., Designing An Improved Transition Metal Phosphide Catalyst for Hydrogen Evolution Using Experimental and Theoretical Trends. *Energy Environ. Sci.* **2015,** *8*, 3022-3029.

(2) Wang, X.-D.; Xu, Y.-F.; Rao, H.-S.; Xu, W.-J.; Chen, H.-Y.; Zhang, W.-X.; Kuang, D.-B.; Su, C.-Y., Novel Porous Molybdenum Tungsten Phosphide Hybrid Nanosheets on Carbon Cloth for Efficient Hydrogen Evolution. *Energy Environ. Sci.* **2016,** *9*, 1468-1475.

(3) Li, D.; Xing, Y.; Yang, R.; Wen, T.; Jiang, D.; Shi, W.; Yuan, S., Holey Cobalt–Iron Nitride Nanosheet Arrays as High-Performance Bifunctional Electrocatalysts for Overall Water Splitting. *ACS Appl. Mater. Interfaces* **2020,** *12*, 29253-29263.

(4) Yu, T.; Xu, Q.; Qian, G.; Chen, J.; Zhang, H.; Luo, L.; Yin, S., Amorphous $CoO_x$-Decorated Crystalline $RuO_2$ Nanosheets as Bifunctional Catalysts for Boosting Overall Water Splitting at Large Current Density. *ACS Sustain. Chem. Eng.* **2020,** *8*, 17520-17526.

(5) Wei, Y.; Zou, P.; Yue, Y.; Wang, M.; Fu, W.; Si, S.; Wei, L.; Zhao, X.; Hu, G.; Xin, H. L., One-Pot Synthesis of B/P-Co-Doped Co-Mo Dual-Nanowafer Electrocatalysts for Overall Water Splitting. *ACS Appl. Mater. Interfaces* **2021,** *13*, 20024-20033.

(6) Mishra, I. K.; Zhou, H.; Sun, J.; Qin, F.; Dahal, K.; Bao, J.; Chen, S.; Ren, Z., Hierarchical CoP/$Ni_5P_4$/CoP Microsheet Mrrays as A Robust pH-Universal

Electrocatalyst for Efficient Hydrogen Generation. *Energy Environ. Sci.* **2018,** *11*, 2246-2252.